Available online at www.sciencedirect.com
ScienceDirect
Geochimica et Cosmochimica Acta 210 (2017) 42–58
Geochimica et Cosmochimica Acta
www.elsevier.com/locate/gca

# Transient deep-water oxygenation in the early Cambrian Nanhua Basin, South China

Meng Cheng [a], Chao Li [a,*], Lian Zhou [b], LianJun Feng [c], Thomas J. Algeo [a,b,d], FeiFei Zhang [e], Stephen Romaniello [e], ChengSheng Jin [a], HongFei Ling [f], ShaoYong Jiang [b,f]

[a] *State Key Laboratory of Biogeology and Environmental Geology, China University of Geosciences, Wuhan 430074, China*
[b] *State Key Laboratory of Geological Processes and Mineral Resources, China University of Geosciences, Wuhan 430074, China*
[c] *Institute of Geology and Geophysics, Chinese Academy of Sciences, Beijing 100029, China*
[d] *Department of Geology, University of Cincinnati, Cincinnati 45221-0013, USA*
[e] *School of Earth and Space Exploration, Arizona State University, Tempe 85287, USA*
[f] *State Key Laboratory for Mineral Deposits Research, Department of Earth Sciences, Nanjing University, Nanjing 210093, China*

Received 23 November 2016; accepted in revised form 20 April 2017; available online 27 April 2017

**Abstract**

Many late Neoproterozoic to early Cambrian fossils of multicellular eukaryotes, including those of benthic animals, are found preserved under anoxic and even euxinic bottom-water conditions, which is contradictory to the consensus that oxygen is essential to eukaryotes. To investigate this conundrum, we conducted an integrated study of iron speciation, redox-sensitive trace elements, and Mo isotopes ($\delta^{98}$Mo) on the black shale interval of the lower Cambrian Hetang Formation (~535–521 Ma) at Lantian, South China, in which benthic sponge fossils are abundant in the lower member (LM) but absent in the upper member (UM). Iron speciation data point to uniformly anoxic-ferruginous conditions in the LM and euxinic conditions in the UM, whereas the trace-element and $\delta^{98}$Mo data show greater secular variation in redox conditions. The LM shows higher mean trace element concentrations (Mo: 108 ppm, U: 36 ppm, V: 791 ppm) and lower and more variable $\delta^{98}$Mo (+0.13 to +1.76‰) relative to the UM (Mo: 45 ppm, U: 18 ppm, V: 265 ppm, $\delta^{98}$Mo: +1.59 to +1.67‰), and ratios of redox-sensitive trace element concentrations to total organic carbon are significantly more variable and higher on average in the LM relative to the UM. The appearance of sponge fossils and lower $\delta^{98}$Mo values correlate strongly with gray (i.e., lighter-colored) layers in the LM. These patterns can best be interpreted as recording mainly euxinic conditions throughout deposition of the study units, with more intense background euxinia in the LM relative to the UM, but also with frequent transient oxygenation events in the LM that do not appear in the UM. The transient oxygenation events of the LM led to the initial colonization of the deep Nanhua Basin by sponges, and the termination of these events in the UM caused sponge faunas to disappear until a general rise in $O_2$ levels later in the Cambrian permitted their return to deeper-water habitats. Our study also illustrates that multiple geochemical and paleobiological proxies exhibit different responses in 'poikiloredox' environments (i.e., characterized by small-scale spatial and high-frequency temporal variations), which can lead to apparent contradictions between metazoan fossil occurrences and their inferred watermass redox conditions.


*Keywords:* Mo isotope; Iron speciation; Trace elements; Sponges; Metazoan; Redox

* Corresponding author.
*E-mail address:* chaoli@cug.edu.cn (C. Li).

http://dx.doi.org/10.1016/j.gca.2017.04.032
0016-7037/

## 1. INTRODUCTION

Animals generally have a strong physiological requirement for oxygen (Knoll and Carroll, 1999; Sperling et al., 2015a) and a limited tolerance for hydrogen sulfide ($H_2S$) (Grice et al., 2005). $H_2S$ forms through microbial sulfate reduction in oxygen-depleted environments, with even low levels being toxic to most eukaryotic organisms. For these reasons, it has been widely argued that an increase in oxygen levels in the atmosphere-ocean system was a necessary precursor to the diversification and spread of metazoans in marine systems prior to and during the early Cambrian (e.g., Knoll and Carroll, 1999; Chen et al., 2015; Sperling et al., 2015b; Jin et al., 2016; Zhang and Cui, 2016). Conversely, expanded oceanic euxinia is widely regarded to have been an important cause of mass extinction events in Earth history (e.g., Wignall and Twitchett, 1996; Grice et al., 2005; Wille et al., 2008; Li et al., 2010).

An apparent contradiction has been observed in Neoproterozoic-Cambrian strata, in which abundant well-preserved fossils have been found apparently in-situ in facies inferred to have been anoxic or even euxinic (e.g., Xiao et al., 2005; Yuan et al., 2011). For instance, the early Cambrian (~529–519 Ma) Niutitang Biota (also known as the Hetang biota), which includes benthic sponges, coelenterates, mollusks, and algae, developed widely in the Nanhua Basin from shallow shelf to deep basin settings, despite the generally anoxic or euxinic conditions of the latter (Jin et al., 2016). Similar contradictions, i.e., abundant eukaryotic fossils in strongly reducing facies, have been reported for the Neoproterozoic (<635 Ma) Lantian (Yuan et al., 2011) and (~560–551 Ma) Miaohe biotas (Li et al., 2015b).

Multiple explanations have been proposed to account for the presence of metazoan fossil assemblages in anoxic/euxinic environments. The hypothesis that these animals lived in the oxic surface layer is refuted by their epifaunal habit (Yuan et al., 2002; Xiao et al., 2005)—there is little doubt that they lived in the bottom waters yielding redox proxy evidence of anoxic/euxinic conditions. Furthermore, many sponges show a close association with microorganisms such as archaea, bacteria, cyanobacteria, yeasts, dinoflagellates, and diatoms, some of which were obligate anaerobes (Moya et al., 2008). However, as the microbial associates often occur intercellularly in the sponge mesohyl (Moya et al., 2008), their association also cannot account for the appearance of sponges in anoxic/euxinic environments. Recently, the hypothesis of short-term oxygenation events was advanced for the Hetang sponges by Zhou and Jiang (2009) as well as for the Ediacaran Lantian Biota by Guan et al. (2014), although without strong empirical support. In general, direct evidence for the existence of oxic conditions in the anoxia-dominated Neoproterozoic-Cambrian oceans is still limited. The difficulty is that, owing to the limited oxygen requirements of early animals, even minor oxygenation events may have permitted transient colonization of normally anoxic environments (Mills et al., 2014), yet common redox proxies such as iron speciation and redox sensitive trace elements (RSTEs) may be sluggish in responding to such transient redox perturbations, and brief oxygenation events may have left behind little to no sedimentary signature.

Molybdenum isotopes ($\delta^{98}$Mo) in organic-rich black shales may uniquely have the ability to capture transient oxygenation events in anoxia-dominated ancient oceans. Sedimentary $\delta^{98}$Mo has been widely applied as a global-ocean redox proxy in euxinic facies, as it is influenced by the overall mass balance of oceanic Mo (Arnold et al., 2004; Dahl et al., 2010; Chen et al., 2015; Kendall et al., 2015). However, for this application to be successful, aqueous Mo must be taken up quantitatively by the sediment, which is most commonly the case when aqueous $H_2S$ concentrations ($[H_2S]_{aq}$) remain uniformly high (Neubert et al., 2008; Gordon et al., 2009; Cheng et al., 2016). In the modern ocean, this condition is met primarily in restricted marine basins such as the Black Sea. If this condition is not met, then sedimentary $\delta^{98}$Mo signatures may reflect local redox variations (Poulson et al., 2006) or, in some cases, the fraction of total time during which euxinia existed at a depositional site (Cheng et al., 2016). In this case, $\delta^{98}$Mo may prove to be a useful proxy for exploring the small-scale redox evolution of ancient oceans. For example, the $\delta^{98}$Mo of weakly euxinic Little Ice Age sediments in the Black Sea may have been controlled by variation in sulfide concentrations (Arnold et al., 2012), and the $\delta^{98}$Mo of suboxic sediments of the Cambrian Yangjiaping section may have been controlled by development of a Mn-Fe shuttle (Cheng et al., 2016). The $\delta^{98}$Mo of ancient marine sediments may have been more susceptible to local watermass redox influences owing to generally low sulfate concentrations in Neoproterozoic-Cambrian oceans (Algeo et al., 2015) and to greater Fe availability (Canfield et al., 2008), resulting in lower $[H_2S]_{aq}$.

In this study, we conducted an integrated investigation of Mo isotopes, iron speciation, and RSTEs on the black shale interval (Unit II) of the lower Cambrian Hetang Formation in the Lantian section, in which sponge fossils are abundant in the lower member (LM) but absent in the upper member (UM). By analyzing multiple redox proxies in the sponge-bearing LM and the non-sponge-bearing UM, our goal is to elucidate the relationship between redox conditions and metazoan colonization of the deep Nanhua Basin in the early Cambrian. As an additional outcome, we also intend to provide insights into the response of multiple geochemical proxies to 'poikiloredox' conditions (i.e., as in an environment characterized by small-scale spatial and high-frequency temporal redox variations).

## 2. GEOCHEMICAL PROXIES USED IN THIS STUDY

### 2.1. Mo isotopes

Molybdenum isotopes are evolving as a powerful proxy to track local and global ocean redox conditions. Most seawater Mo is sourced from continental weathering and is removed via burial in authigenic phases under oxic, suboxic, or euxinic conditions (Siebert et al., 2003; Cheng et al., 2015). The largest Mo isotopic fractionation of 3‰ occurs in oxic waters during slow adsorption onto Mn oxides (Barling and Anbar, 2004). The fractionation of sediment

$\delta^{98}$Mo relative to seawater $\delta^{98}$Mo is limited under the condition of quantitative precipitation of aqueous Mo, which requires $[H_2S]_{aq}$ to exceed a threshold value of ~11 μM on a timescale of years because of the slow kinetics of the conversion process (Erickson and Helz, 2000), but significant Mo-isotope fractionation can develop at persistently low $[H_2S]_{aq}$ or when $[H_2S]_{aq}$ fluctuates strongly (Neubert et al., 2008). In this regard, a positive linear relationship between $[H_2S]_{aq}$ concentrations and sediment $\delta^{98}$Mo has been reported for modern aqueous systems with $H_2S < 11$ μM (Neubert et al., 2008). Thus, high-frequency fluctuations in $[H_2S]_{aq}$ concentrations are likely to be reflected in sediment $\delta^{98}$Mo signatures.

### 2.2. Iron speciation

Iron speciation can serve as a paleo-redox proxy owing to the redox-related re-distribution of iron in the ocean. Most iron transported from continents by rivers is precipitated quickly on continental shelves (Raiswell and Canfield, 2012). As continental shelves are also areas of active organic carbon production, anoxia commonly develops in sediment pore waters, leading to diffusion of soluble reduced Fe back into the water column (Scholz et al., 2016). This process preferentially affects highly reactive iron ($Fe_{HR}$), which can migrate into deep-water settings as $Fe^{2+}$ via the oxygen minimum zone (OMZ) or as nano-oxides via oxic waters (Raiswell and Canfield, 2012). In euxinic facies in which free $H_2S$ exists, reactive iron forms pyrite and is removed to the sediment. Consequently, anoxic sediments show elevated $Fe_{HR}/Fe_T$ ($Fe_T$: total iron), and euxinic sediments show elevated $Fe_{py}/Fe_{HR}$ ratios ($Fe_{py}$: pyrite iron) (Lyons and Severmann, 2006). Statistically, $Fe_{HR}/Fe_T < 0.22$ indicates oxic conditions and $Fe_{HR}/Fe_T > 0.38$ anoxic conditions. Further, when anoxia is indicated, $Fe_{py}/Fe_{HR} < 0.7$ and $Fe_{py}/Fe_{HR} > 0.7$ suggest ferruginous and euxinic conditions, respectively (Poulton and Canfield, 2011). These thresholds are most robust for samples containing $Fe_T > 0.5\%$, and caution must be exercised at lower $Fe_T$ concentrations (Clarkson et al., 2014).

### 2.3. Redox-sensitive trace elements (Mo, U and V)

Mo is conservative as molybdate ($MoO_4^{2-}$) in oxic waters despite slow adsorption onto Mn oxides, but in the presence of $H_2S$ (i.e., in a euxinic water column or sulfidic porewaters) $MoO_4^{2-}$ is converted to more particle-reactive thiomolybdates ($MoO_{4-x}S_x^{2-}$, $x = 1$–$4$), which can then be efficiently removed to the sediment via adsorption onto organic matter or formation of authigenic Fe-Mo-S minerals, resulting in high sedimentary Mo concentrations (Algeo and Lyons, 2006; Dahl et al., 2013). U and V are conservative in oxic waters as $U^{6+}$ and $V^{5+}$, respectively (Tribovillard et al., 2006; Algeo and Tribovillard, 2009). Both Mo and V are strongly adsorbed onto Fe-Mn oxyhydroxides whereas U is not; consequently, crossplots of $Mo_{EF}$ versus $U_{EF}$ have been proposed as a proxy for recognition of the Fe-Mn shuttle effect, which leads to strong enrichment of Mo without a corresponding enrichment of U (Algeo and Tribovillard, 2009). $U^{6+}$ and $V^{5+}$ are reduced to $U^{4+}$ and $V^{4+}$, respectively, around the $Fe^{3+}$ to $Fe^{2+}$ transition (i.e., under "suboxic" conditions). Free $H_2S$ leads to reduction of $V^{4+}$ to $V^{3+}$ and enhances the reduction of $U^{6+}$ to $U^{4+}$, resulting in higher concentrations of these RSTEs in euxinic facies (Algeo and Lyons, 2006; Tribovillard et al., 2006). Thus, suboxic bottom-water conditions are generally characterized by modest U and V enrichments with little to no Mo enrichment, whereas euxinic conditions are characterized by strong enrichments of all three RSTEs with Mo commonly showing the largest enrichment factors.

## 3. GEOLOGICAL SETTING

The Nanhua Basin developed as a failed intracratonic rift basin between the Yangtze and Cathaysia blocks of the South China Craton during the breakup of the Rodinia supercontinent at ~820 Myr (Wang and Li, 2003). By the early Cambrian, it was located at ~20°N paleolatitude (Fig. 1A) (Zhang et al., 2015). Paleogeographic reconstructions show a transition from shelf settings to the northwest to basinal settings to the southeast (modern coordinates), with the Lantian section located in the basinal area (Fig. 1B) (Goldberg et al., 2007). At Lantian, the lower Cambrian Hetang Formation conformably overlies the Piyuancun Formation (which contains the Precambrian/Cambrian boundary) and underlies the lower Cambrian Dachenling Formation (Figs. 1C, and 2A). It consists of four lithostratigraphic units (in ascending order): Unit I is a ~68-m layer dominated by siliceous-carbonaceous mudstone and shale with phosphorite nodules (Fig. 2B); Unit II is a ~30-m organic-rich black shale layer; Unit III is a ~110-m unit of siliceous-carbonaceous shale; and Unit IV is a ~110-m carbonaceous shale layer with carbonate nodules (Fig. 2C) (Zhou and Jiang, 2009). Mainly based on SSFs (small shelly fossils) and trilobites, the age of the Unit II is constrained to the Meishucunian-Qiongzhusian (~535–521 Ma) (see detail in Xiao et al., 2005).

In this study, we focused on the black shales of Unit II at Lantian. We collected a total of 31 samples at a spacing of ~1 m through a stratigraphic interval representing ~14 Myr. The study interval accumulated at an average sedimentation rate of 0.22 cm $kyr^{-1}$ (i.e., 31 m/14 Myr), with sample spacing representing a temporal resolution of ~450 kyr/sample. This timescale is close to the residence times of Mo and U in modern seawater (~780 kyr and 450 kyr, respectively; Algeo and Tribovillard, 2009), but it may be longer than the residence times of these elements in early Cambrian seawater, when more widespread anoxia in the oceans would have drawn down their seawater inventory. Individual samples were taken from horizons ~2–5 cm in thickness, each representing ~10–20 kyr of depositional time.

In Unit II and adjacent correlative strata regionally, many sponge fossils have been found in the lower half but not in the upper half of the unit (Yuan et al., 2002; Xiao et al., 2005), and these sponges were typical of deep-water communities (Botting and Peel, 2016). For this reason, we divide Unit II into a fossil-bearing lower member (LM; from 0 m to 16 m) and a non-fossil-bearing upper member (UM; from 16 m to 31 m) (Fig. 1C). In the LM,

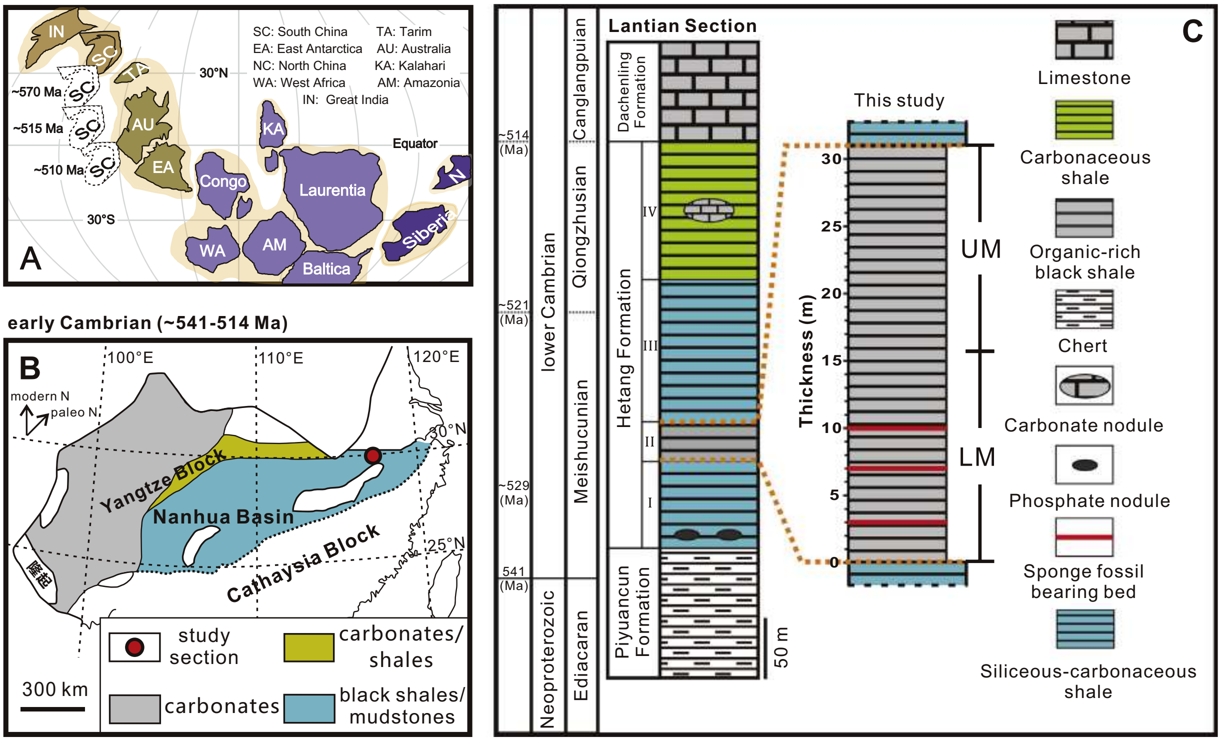


Fig. 1. Geological setting of the Lantian section. (A) Global paleogeography in early Cambrian. Modified from Zhang et al. (2015). (B) Paleogeography of South China in early Cambrian. Modified from Goldberg et al. (2007). (C) Generalized stratigraphy of the Lantian section.

at least eleven species of articulated demosponges and hexactinellids are preserved (Fig. 2D–G), with some sponges up to ~1 m in diameter (Yuan et al., 2002; Xiao et al., 2005). In contrast, bilaterians (including orthothecid hyoliths and bivalved arthropods) are much smaller (<0.5 cm) (Yuan et al., 2002). These fossil assemblages accumulated *in situ*, and most taxa are inferred to have had a *benthic habit* (Yuan et al., 2002; Xiao et al., 2005). Similar occurrences of fossils are known from other sections regionally (Xiao et al., 2005), and related taxa are known from coeval strata in Siberia and Greenland (Botting and Peel, 2016). The three main fossil-bearing layers in the LM are at ~3, ~7, and ~10 m above the base of the section. The fossiliferous intervals consist of several closely-spaced (i.e., a few mm apart) fossil-bearing layers with alternating black and gray color (Fig. 2H). Fossils are preferentially concentrated in the gray-colored layers, although larger fossils can cut across several black-gray layer pairs.

## 4. MATERIALS AND METHODS

All samples were collected from a quarry outcrop near Lantian Village, Xiuning County, Anhui Province (29° 53′36″N, 118°03′52″E) (Fig. 2A). In collecting samples, weathered surfaces, veins, and macroscopic pyrite nodules were avoided. Each sample consisted of a large block (>500 g), from which only the freshest portions (~50 g) were taken and crushed to powder of >200 mesh (i.e., finer than 0.075 mm) for chemical analyses.

To remove inorganic carbon in the samples, the sample powders were immersed repeatedly in hydrochloric acid and rinsed. TOC concentrations were determined via online combustion in a high-frequency infrared carbon and sulfur analyzer (CS-902 G/T, Beijing Wanlianda Inc.).

Iron hosted by different minerals including oxides ($Fe_{ox}$), magnetite ($Fe_{mag}$), and carbonates ($Fe_{carb}$) was extracted using a sequential extraction procedure developed by Poulton and Canfield (2005). Extracted iron concentrations were determined using an atomic absorption spectrometer (AAS) with a RSD of <5%. Fe in pyrite ($Fe_{py}$) was extracted using the chromium reduction method of Canfield et al. (1986), and the concentration of $Fe_{py}$ was calculated stoichiometrically assuming a 1:2 Fe:S molar ratio in pyrite. Total iron and Al concentrations were determined using an inductively coupled plasma optical emission spectrometry (ICP-OES) after digestion with $HNO_3$ and HF, with analytical precision of ~10%.

Trace elemental concentrations were determined using an inductively coupled plasma mass spectrometer (ICP-MS, Agilent 7700x). Sample powders were first ashed at ~600 °C for 10 h to remove organic matter. About 50 mg of ashed powder were weighed into a Teflon bomb and then digested with $HNO_3$ and HF at a temperature of 190 °C. Subsequently, the solution was diluted to 100 g with 2% $HNO_3$ and analyzed. Three international standards (AGV-2, NHVO-2 and BCR-2) and two Chinese national standards (GSR-5 and GSR-6) were used to monitor data quality, yielding an analytical precision of ~10%. Enrich-

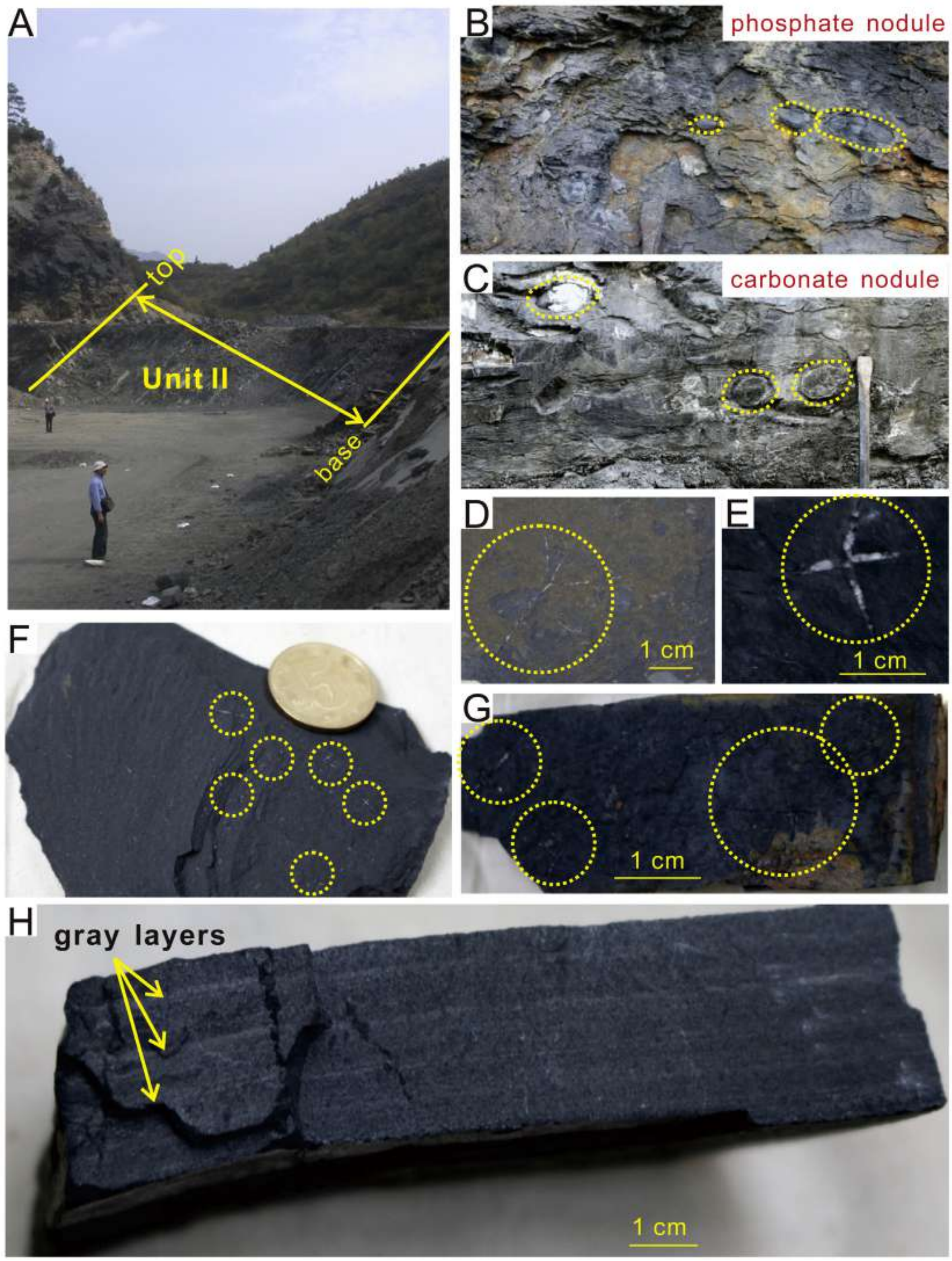


Fig. 2. Photographs of the Hetang Formation in the Lantian section. (A) Unit II black shales in quarry outcrop. (B) Phosphorite nodules in lower Unit I. (C) Carbonate nodules in Unit IV. (D and E) Sponge fossils at ~7 m and ~10 m in study section (for a detailed description, see Xiao et al. (2005)). (F and G) Concentrated sponge fossils in thin gray beds at ~3 m and ~7 m. (H) Lithological variation (alternating gray and black layers) in ~3 m of strata.

ment factors (EF) for trace elements (X, where X is Mo, U or V) relative to upper continental crust (UCC) (McLennan, 2001) were calculated as:

$$X_{EF} = (X/Al)_{sample}/(X/Al)_{UCC} \quad (1)$$

Mo isotopes were analyzed using the method described by Cheng et al. (2016). A $^{97}Mo$-$^{100}Mo$ double spike was added to the ashed sample powders, which were then digested using the same process as for trace elements. Mo was separated from this solution using anion resin (GPM-

1M, Bio-Rad) and cation resin (AG50W-X8, Bio-Rad) and analyzed using a Neptune Plus MC-ICP-MS (Thermo Fisher Scientific). The long-term external reproducibility for Mo isotope measurements of standard reference materials is better than 0.05‰. Results are reported in per mille variation of $\delta^{98}$Mo relative to the Johnson Matthey Company (JMC) Specpure Mo plasma standard (lot 602332B):

$$\delta^{98}\mathrm{Mo} = ({}^{98/95}\mathrm{Mo}_{\mathrm{sample}}/{}^{98/95}\mathrm{Mo}_{\mathrm{JMC}} - 1) \times 1000 \quad (2)$$

Nägler et al. (2013) proposed that NIST SRM 3134 ($\delta^{98}\mathrm{Mo} = +0.25$‰) be adopted as an international Mo isotope standard. Using the JMC standard, analysis of NIST SRM 3134 at multiple laboratories yielded a value of $+0.27 \pm 0.06$ (Goldberg et al., 2013). All Mo isotope ratios reported in this study were re-calculated to NIST SRM $3134 = +0.25$‰ by subtraction of 0.02‰ from measured values.

## 5. RESULTS

All data from this study are listed in Table A1, and key geochemical results are summarized in Fig. 3. $Fe_T$ ranges from 0.7% to 4.0% with a mean of ~2.0%. $Fe_{HR}/Fe_T$ ratios are uniformly high, ranging from 0.67 to 1.00. $Fe_{py}/Fe_{HR}$ ratios are generally higher in the UM ($0.75 \pm 0.08$) (mean $\pm\, \sigma$) than in the LM ($0.65 \pm 0.10$). TOC values are generally high, although much higher in the LM (8.5–14.3%) than in the UM (4.1–6.5%). Mo, U and V all show significant enrichment relative to UCC and are generally higher in the LM (Mo: 19–288 ppm, U: 2–92 ppm, V: 183–1916 ppm) than in the UM (Mo: 16–58 ppm, U: 10–28 ppm, V: 95–521 ppm). $\delta^{98}$Mo values show a broad range in the LM from +0.11‰ to +1.76‰, but a limited range in the UM from +1.59‰ to +1.67‰.

## 6. DISCUSSION

### 6.1. General redox interpretations for Lantian

Iron speciation and RSTE data indicate anoxic bottom-water conditions for both the LM and UM. In Unit II, all samples yielded $Fe_T$ concentrations > 0.5%, providing a valid basis for iron speciation analysis (Clarkson et al., 2014). $Fe_{HR}/Fe_T$ ratios range from 0.67 to 1.00, which are all higher than the threshold value of 0.38 for anoxic conditions (Fig. 3) (Poulton and Canfield, 2011). Mo, U and V show moderate to strong enrichments relative to UCC ($Mo_{EF}$: 20–497, $U_{EF}$: 3–111, $V_{EF}$: 2–92) (Fig. 3), also suggesting anoxic bottom waters. In summary, the proxies of $Fe_{HR}/Fe_T$ and RSTEs are consistent in indicating anoxic bottom-water conditions for the whole interval of Unit II. Consequently, our iron speciation and RSTE data pose a contradiction in that the benthic animals preserved in Unit II seemingly lived in anoxic waters.

With regard to distinguishing euxinic and ferruginous conditions, iron speciation and RSTE data yielded contradictory results. Although $Fe_{HR}/Fe_T$ ratios are consistently >0.38 throughout Unit II, $Fe_{py}/Fe_{HR}$ ratios are generally <0.7 in the LM but >0.7 in the UM, suggesting ferruginous and euxinic conditions, respectively (Fig. 3). On the other hand, RSTEs show higher concentrations in the LM than in the UM, e.g., >100 ppm versus >25 ppm for Mo, which indicate more intensely euxinic conditions in the former (Fig. 3). In modern anoxic facies, Mo concentrations of ~25–100 ppm and >100 ppm have been interpreted as evidence of intermittent versus sustained bottom-water euxinia, respectively (Scott and Lyons, 2012). Lower $Fe_{py}/Fe_{HR}$ values in the LM are unlikely to have been a result of deep oxidative weathering of pyrite because all Unit-II samples were from a fresh quarry outcrop with only a ~30-m thickness for the Unit II (Fig. 2A). Additional RSTE evidence for this inference will be given in Sections 6.2 and 6.4. Thus, the contradictory redox interpretations yielded by the iron speciation and RSTE data suggest the influence of other factors in addition to watermass redox conditions.

### 6.2. Resolving redox proxy conflicts at Lantian

The discrepant redox interpretations of the iron speciation and RSTE data suggest an anomaly in one proxy or the other. Iron speciation anomalies can develop owing to changes in sedimentation rates, Fe export efficiency from shelves, or the redox conditions of sediment porewaters (Tessin et al., 2016). $Fe_T$ concentrations in the LM ($1.69 \pm 0.82$%) are lower on average than those in the UM ($2.21 \pm 0.73$%), indicating possible low Fe export efficiency during LM deposition. However, an independent T-test shows that the difference in mean $Fe_T$ values between the two members is not significant ($p > 0.05$). Although $Fe_T$ concentrations in the LM vary from 0.7% to 3.8%, most samples show constant $Fe_{py}/Fe_{HR} < 0.7$, excluding low Fe availability as the cause. Al concentrations are higher in the UM ($4.10 \pm 0.67$%) than in the LM ($2.26 \pm 0.75$%) ($p < 0.01$), indicating possible dilution of authigenic elements by detrital siliciclastic inputs. In theory, such dilution will lower $Fe_{HR}/Fe_T$ ratios as more non-reactive Fe is deposited (Lyons and Severmann, 2006), but it will not affect $Fe_{py}/Fe_{HR}$. In moving from the LM to the UM, $Fe_{HR}/Fe_T$ values remain relatively constant, whereas $Fe_{py}/Fe_{HR}$ values increase from $0.65 \pm 0.10$ to $0.75 \pm 0.08$ ($p < 0.01$). This pattern argues strongly against an effect linked to siliciclastic dilution. Oxidation of pyrite after deposition can change the distribution of Fe in highly reactive species, leading to lower $Fe_{py}/Fe_{HR}$ (Li et al., 2012). However, oxidation of pyrite will simultaneously result in the loss of RSTEs (Large et al., 2014), this mechanism cannot explain higher RSTE concentrations in the LM. However, a syndepositional oxidation process is still possible and we will discuss this further in Section 6.4.

The alternative is that RSTE anomalies are responsible for the discrepancy in redox proxy results noted above. Strong enrichment of Mo in marine sediments, besides the effect of $H_2S$, can be the result of adsorption of Mo onto sinking Fe-Mn particulates, i.e., the "particulate shuttle" effect of Algeo and Tribovillard (2009). This process leads to higher $Mo_{EF}$ relative to $U_{EF}$ for intermediate levels of RSTE enrichment. At higher levels of RSTE enrichment (e.g., $Mo_{EF} > 100$ and $U_{EF} > 30$), the particulate shuttle and open-marine trends converge, impeding recognition

Table A1
Geochemical data for Unit II of lower Hetang Formation in Lantian section, South China.

| Member[a] | Sample | Depth (m) | TOC (wt%) | $Fe_T$ (wt%) | Al (wt%) | $Fe_{carb}$ (wt%) | $Fe_{ox}$ (wt%) | $Fe_{mag}$ (wt%) | $Fe_{py}$ (wt%) | $Fe_{HR}/Fe_T$ | $Fe_{py}/Fe_{HR}$ | $\delta^{98}Mo$[b] (‰) | $\delta^{98}Mo$[c] (‰) | Mo (ppm) | U (ppm) | V (ppm) |
|---|---|---|---|---|---|---|---|---|---|---|---|---|---|---|---|---|
| UM | H73 | 31.0 | 4.10 | 2.00 | 4.80 | 0.40 | 0.30 | 0.00 | 1.30 | 1.00 | 0.65 | 1.69 | 1.67 | 50.06 | 10.49 | 286.29 |
| UM | H72 | 30.0 | 4.80 | 1.90 | 4.70 | 0.30 | 0.50 | 0.00 | 1.10 | 1.00 | 0.58 | | | 45.80 | 15.53 | 420.52 |
| UM | H70 | 28.0 | 4.60 | 1.20 | 4.70 | 0.00 | 0.10 | 0.00 | 0.90 | 0.83 | 0.90 | | | 48.05 | 12.17 | 499.53 |
| UM | H69 | 27.0 | 4.10 | 2.30 | 4.20 | 0.00 | 0.50 | 0.00 | 1.30 | 0.78 | 0.72 | | | 56.42 | 16.59 | 520.53 |
| UM | H68 | 26.0 | 4.70 | 2.40 | 5.10 | 0.00 | 0.60 | 0.00 | 1.40 | 0.83 | 0.70 | | | 35.81 | 19.38 | 361.57 |
| UM | H67 | 25.0 | 5.30 | 2.60 | 4.20 | 0.00 | 0.40 | 0.00 | 1.70 | 0.81 | 0.81 | 1.69 | 1.67 | 15.91 | 11.82 | 176.85 |
| UM | H66 | 24.0 | 5.80 | 2.10 | 3.40 | 0.00 | 0.50 | 0.00 | 1.30 | 0.86 | 0.72 | 1.69 | 1.67 | 54.58 | 26.80 | 216.81 |
| UM | H65 | 23.0 | 4.70 | 2.00 | 4.00 | 0.00 | 0.30 | 0.00 | 1.30 | 0.80 | 0.81 | | | 46.04 | 18.76 | 233.22 |
| UM | H64 | 22.0 | 6.10 | 4.00 | 4.40 | 0.00 | 0.50 | 0.10 | 2.90 | 0.88 | 0.83 | | | 26.46 | 19.06 | 194.84 |
| UM | H63 | 21.0 | 4.60 | 3.40 | 4.60 | 0.00 | 0.60 | 0.00 | 2.40 | 0.88 | 0.80 | 1.67 | 1.65 | 49.19 | 14.34 | 195.30 |
| UM | H62 | 20.0 | 5.50 | 1.80 | 3.10 | 0.10 | 0.30 | 0.00 | 1.10 | 0.83 | 0.73 | | | 42.46 | 22.28 | 185.24 |
| UM | H61 | 19.0 | 4.50 | 1.90 | 3.80 | 0.00 | 0.40 | 0.00 | 1.00 | 0.74 | 0.71 | | | 43.21 | 15.43 | 94.96 |
| UM | H60 | 18.0 | 5.30 | 1.90 | 3.30 | 0.00 | 0.40 | 0.00 | 1.10 | 0.79 | 0.73 | | | 52.50 | 27.59 | 166.06 |
| UM | H59 | 17.0 | 6.50 | 1.50 | 3.10 | 0.00 | 0.30 | 0.00 | 1.00 | 0.87 | 0.77 | 1.61 | 1.59 | 58.20 | 19.10 | 155.14 |
| LM | H58 | 16.0 | 9.40 | 2.40 | 2.90 | 0.20 | 0.50 | 0.00 | 1.30 | 0.83 | 0.65 | | | 48.33 | 23.27 | 248.93 |
| LM | H57 | 15.0 | 8.50 | 1.60 | 2.80 | 0.10 | 0.50 | 0.00 | 0.80 | 0.88 | 0.57 | | | 65.89 | 33.32 | 183.44 |
| LM | H56 | 14.0 | 10.50 | 2.40 | 3.00 | 0.20 | 0.50 | 0.00 | 1.40 | 0.88 | 0.67 | | | 55.10 | 37.34 | 241.30 |
| LM | H55 | 13.0 | 10.70 | 1.80 | 2.30 | 0.20 | 0.40 | 0.00 | 0.90 | 0.83 | 0.60 | | | 65.60 | 29.35 | 302.46 |
| LM | H54 | 12.0 | 10.30 | 2.50 | 2.40 | 0.00 | 0.40 | 0.00 | 1.70 | 0.84 | 0.81 | 1.78 | 1.76 | 97.44 | 17.04 | 456.49 |
| LM | H53 | 11.0 | 9.80 | 1.00 | 2.60 | 0.00 | 0.40 | 0.00 | 0.50 | 0.90 | 0.56 | | | 123.41 | 29.38 | 1380.96 |
| LM | H52 | 10.0 | 10.10 | 1.90 | 2.90 | 0.20 | 0.70 | 0.00 | 1.00 | 1.00 | 0.53 | 0.28 | 0.26 | 173.33 | 24.21 | 1915.77 |
| LM | H51 | 9.0 | 13.00 | 0.70 | 0.80 | 0.00 | 0.20 | 0.00 | 0.40 | 0.86 | 0.67 | | | 64.72 | 30.90 | 979.62 |
| LM | H50 | 8.0 | 11.30 | 3.80 | 3.80 | 0.60 | 0.70 | 0.00 | 2.40 | 0.97 | 0.65 | 1.64 | 1.62 | 287.54 | 92.24 | 798.70 |
| LM | H49 | 7.0 | 14.10 | 0.70 | 1.20 | 0.00 | 0.20 | 0.00 | 0.40 | 0.86 | 0.67 | 0.72 | 0.70 | 78.45 | 25.54 | 754.78 |
| LM | H47 | 5.0 | 9.10 | 1.20 | 1.60 | 0.10 | 0.30 | 0.00 | 0.50 | 0.75 | 0.56 | 1.22 | 1.20 | 148.25 | 59.69 | 754.26 |
| LM | H46 | 4.0 | 13.50 | 1.30 | 1.60 | 0.30 | 0.40 | 0.00 | 0.60 | 1.00 | 0.46 | | | 124.30 | 41.33 | 1834.16 |
| LM | H45 | 3.0 | 12.00 | 1.20 | 2.10 | 0.00 | 0.20 | 0.00 | 0.70 | 0.75 | 0.78 | 0.13 | 0.11 | 106.85 | 27.02 | 1725.65 |
| LM | H44 | 2.0 | 12.70 | 1.50 | 2.00 | 0.00 | 0.20 | 0.00 | 0.80 | 0.67 | 0.80 | 1.22 | 1.20 | 121.11 | 44.01 | 440.34 |
| LM | H43 | 1.0 | 11.40 | 2.10 | 2.20 | 0.20 | 0.30 | 0.00 | 1.20 | 0.81 | 0.71 | 1.72 | 1.70 | 141.91 | 52.78 | 325.22 |
| LM | H42 | 0.0 | 14.30 | 0.90 | 2.00 | 0.00 | 0.20 | 0.00 | 0.40 | 0.67 | 0.67 | 0.28 | 0.26 | 18.70 | 1.84 | 319.78 |

[a] LM = lower member; UM = upper member.
[b] Mo isotopic data reported relative to JMC.
[c] Mo isotopic data reported relative to NIST SRM 3134 = 0.25‰.

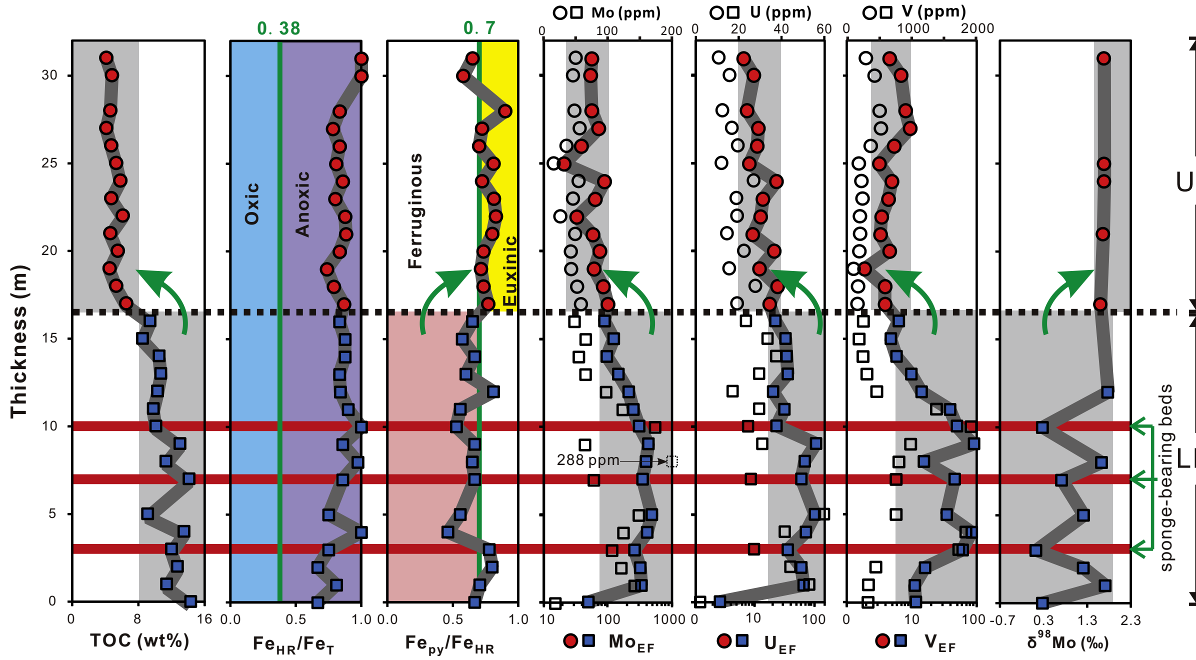

Fig. 3. Chemostratigraphy of Unit II of the Hetang Formation in the Lantian section. LM = lower member, UM = upper member.

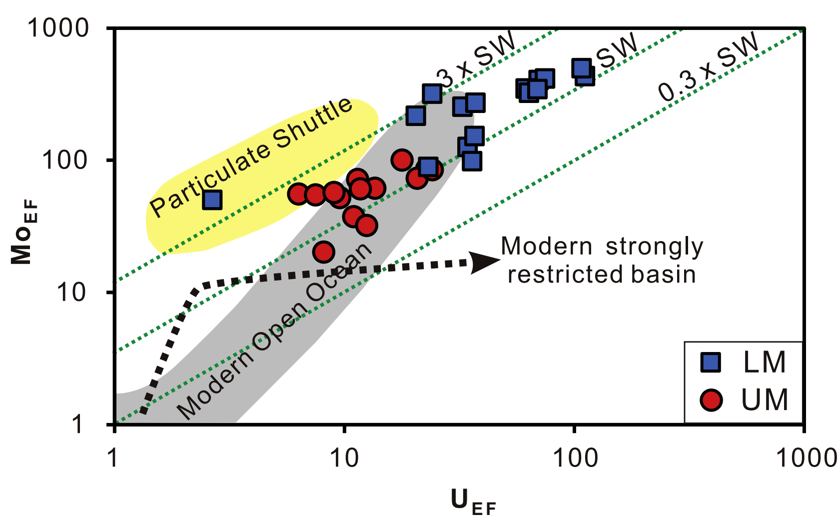

Fig. 4. $Mo_{EF}$ vs. $U_{EF}$ for Unit II of the Hetang Formation in the Lantian section. Particulate shuttle and redox fields are from Algeo and Tribovillard (2009). LM = lower member, UM = upper member.

of influence by a particulate shuttle (Fig. 4) (Algeo and Tribovillard, 2009). At Lantian, many Unit II samples exhibit large $Mo_{EF}$ and $U_{EF}$ (Fig. 3), putting them beyond the particulate shuttle field, although one LM sample with relatively low $U_{EF}$ plots within this field (Fig. 4). It is thus possible that Fe-Mn redox cycling occurred between an oxic ocean-surface layer and an anoxic deep watermass at Lantian, contributing to overall Mo enrichment.

RSTE concentrations are commonly closely linked to sediment TOC content (Algeo and Maynard, 2004; Tribovillard et al., 2006), and higher Mo, U, and V concentrations roughly correspond to higher TOC contents in this study although the correlations are not significant (Fig. 5). Therefore, we calculated RSTE/TOC ratios to normalize for variable TOC content between the LM (8.4–14.3%, mean 11.1%) and UM (4.1–6.5%, mean 5.0%) (Fig. 3). The RSTE/TOC profiles show a reduction in the difference of mean values between the LM and UM (Fig. 6), demonstrating that at least a part of the differences in RSTE concentrations is due to differences in TOC content. However, the RSTE/TOC profiles continue to show higher values and greater sample-to-sample variance in the LM relative to the UM (Fig. 6). One important control on the accumulation of authigenic RSTEs in the sediment is the availability of

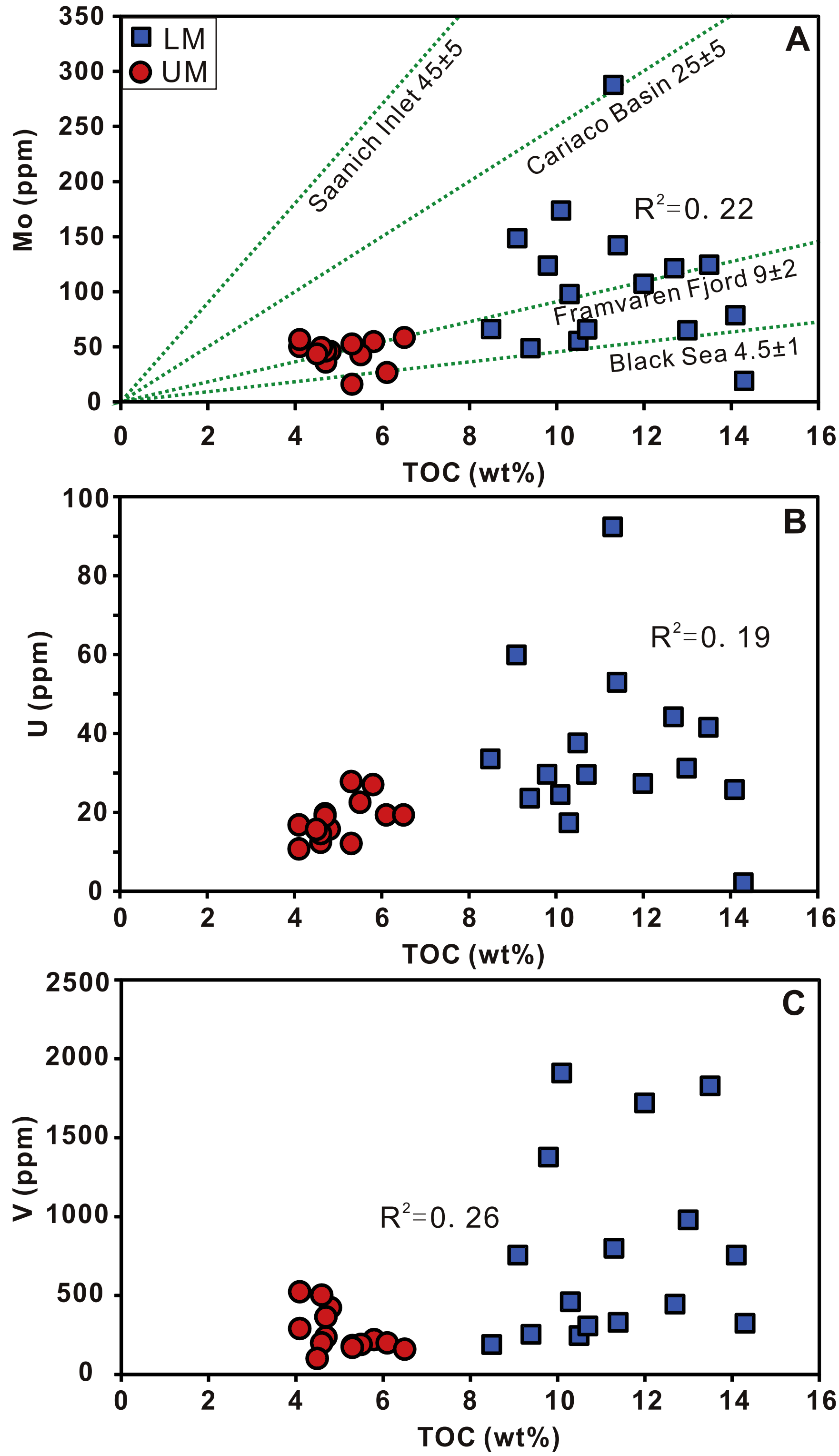


Fig. 5. Mo (A), U (B), V (C) versus TOC for Unit II of the Hetang Formation in the Lantian section. Correlation coefficient ($R^2$) of each element with TOC for the Unit II is provided in each panel for reference. The green dotted lines in panel A represent the average ratios for modern restricted marine basins (Algeo and Lyons, 2006). LM = lower member, UM = upper member.

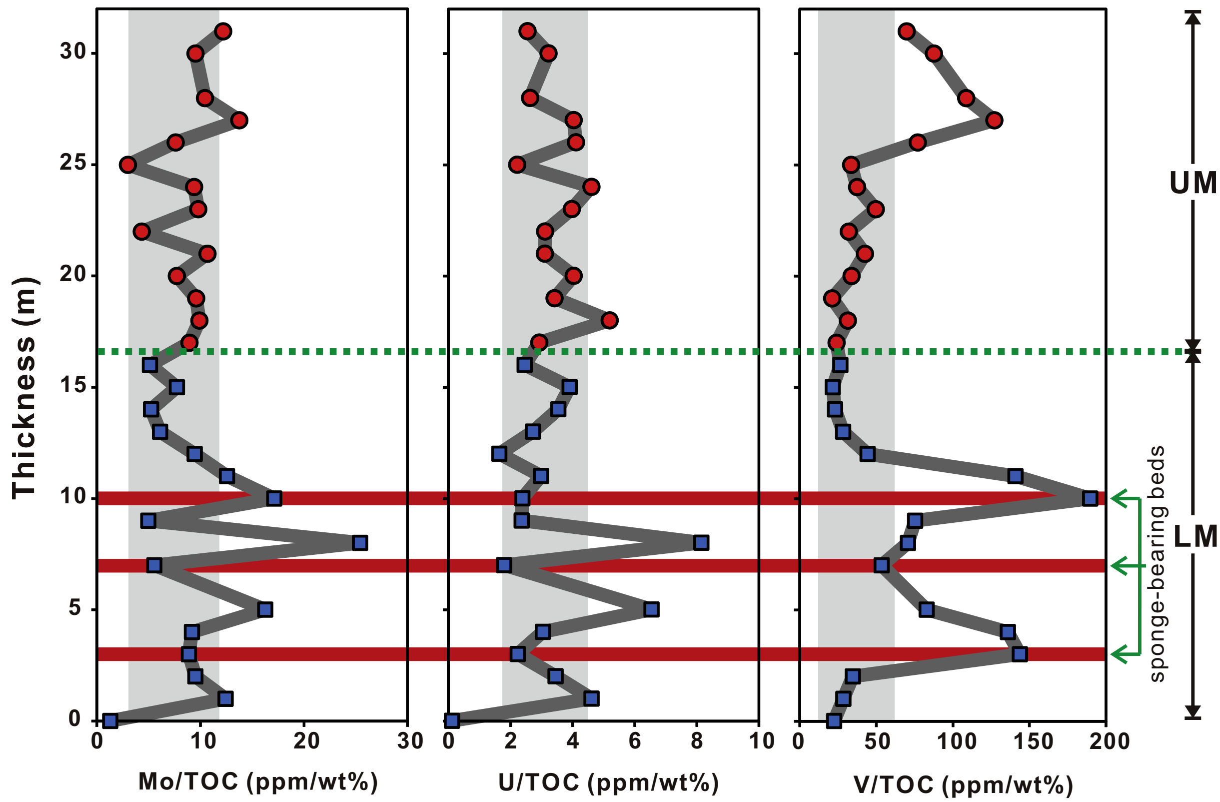


Fig. 6. RSTE/TOC profile for Unit II of the Hetang Formation in the Lantian section. LM = lower member, UM = upper member.

dissolved RSTEs in the water column (Algeo and Rowe, 2012). RSTE/TOC ratios have been widely used as a proxy to track RSTE availability in ancient oceans (e.g., Algeo and Lyons, 2006; Scott et al., 2008). In Unit II, most samples show a relatively uniform RSTE/TOC ratio (gray bars, Fig. 6), consistent with the idea of control by fixed aqueous RSTE concentrations. However, some samples in the LM show distinctly higher RSTE/TOC ratios. We thus infer that these samples are related to differences in RSTE availability during the deposition. This pattern suggests that RSTE availability in the Nanhua Basin was steady during most of the Unit II interval, but increased episodically during deposition of the LM.

There are two principal explanations for episodic increases in aqueous Mo availability in the Nanhua Basin, the first being intermittent deepwater renewal events within a restricted marine basin. The relatively low Mo/TOC ratios of Unit II ($8 \pm 3$ ppm/%) are close to those of modern Framvaren Fjord ($9 \pm 2$ ppm/%; Fig. 5) (Algeo and Lyons, 2006), which might suggest strong basinal restriction. However, the Nanhua Basin is considered to have had an open connection to the global ocean during the early Cambrian (e.g., Jiang et al., 2003), arguing against basinal restriction. In addition, modern strongly silled basins show much lower $Mo_{EF}$ relative to $U_{EF}$ (Algeo and Tribovillard, 2009), which is not observed at Lantian (Fig. 4).

The alternative explanation for episodic increases in aqueous Mo availability is that, because Mo concentrations were generally low in anoxic early Cambrian oceans (Feng et al., 2014; Sperling et al., 2015b; Jin et al., 2016), pulsed increases in dissolved oxygen levels episodically reduced the flux of Mo into anoxic sinks, allowing buildup of seawater Mo concentrations to higher concentrations. Since the removal efficiency of RSTEs into anoxic facies is significantly higher than into oxic facies, the oceanic RSTE reservoir is quite sensitive to the area of seafloor covered by oxygen-deficient waters (Algeo, 2004; Scott et al., 2008). For example, euxinia covering <10% of global seafloor area can cause the oceanic Mo reservoir to decline to negligible levels (Reinhard et al., 2013). We infer that the episodically elevated RSTE/TOC values in the LM (Fig. 6) may reflect episodic global-ocean oxidation events. Although the modern seawater residence time of Mo (~780 kyr) would not allow short-term events of this type, a much shorter residence time during the early Cambrian would have permitted high-frequency variation at timescales shorter than the average interval between our study samples (~450 kyr; Section 3).

### 6.3. Mo-isotope evidence for episodic redox perturbations

The Mo-isotopic compositions of marine sediments can provide information about global-ocean redox conditions (provided that certain conditions are met; see Section 2.1) or local redox conditions (if those conditions are not met). We infer that most of our Mo-isotope dataset reflects global-ocean redox conditions, although a subset of samples shows values consistent with local redox influences.

The Mo-isotope data of Unit II can be divided into two subsets of samples, with the larger subset having relatively high and nearly uniform $\delta^{98}$Mo of ~+1.7‰ (Fig. 3). This subset includes all samples from the UM ($n = 5$) and some samples from the LM ($n = 3$ of 9 total). In order for sediment $\delta^{98}$Mo to reflect the isotopic composition of contemporaneous seawater, uptake of aqueous Mo by the sediment must be quantitative, which is generally the case at higher $[H_2S]_{aq}$ (Erickson and Helz, 2000; Neubert et al., 2008). To date, no proxy is available to constrain $[H_2S]_{aq}$ in ancient seawater. However, if uptake of Mo had been non-quantitative owing to low $[H_2S]_{aq}$, then one would expect to observe high-frequency fluctuations in sediment $\delta^{98}$Mo in response to variations in $[H_2S]_{aq}$ caused by vagaries in the rates of $H_2S$ production and consumption related to organic matter sinking fluxes, sulfate availability, iron inputs, and other factors (Arnold et al., 2012). In fact, the uniformity of $\delta^{98}$Mo for most of our samples implies that any fluctuations of $[H_2S]_{aq}$ in the Lantian depositional environment occurred at concentrations above the threshold for quantitative uptake of Mo by the sediment and, therefore, that a value of +1.7‰ represents that of contemporaneous seawater Mo.

The second subset of Unit II samples, which is found exclusively in the LM (6 of 9 total samples), is characterized by lighter and more variable $\delta^{98}$Mo (Fig. 3). This subset is unlikely to record contemporaneous seawater $\delta^{98}$Mo values. Relative to a baseline $\delta^{98}$Mo value of +1.7‰ (see above), a decline in seawater $\delta^{98}$Mo due to enhanced global-ocean anoxia would have been accompanied by a decrease in the oceanic Mo reservoir size (Wille et al., 2008). However, the Mo concentrations and Mo/TOC ratios in the study samples yielding lighter $\delta^{98}$Mo values are similar to or slightly greater than those for samples exhibiting the baseline $\delta^{98}$Mo value of +1.7‰ (Figs. 3 and 6). Also, the lowest of the measured $\delta^{98}$Mo values in the study samples are even lower than the average crustal $\delta^{98}$Mo of ~+0.4‰ (Voegelin et al., 2014; Breillat et al., 2016; Yang et al., 2017), and seawater $\delta^{98}$Mo cannot go lower than the isotopic composition of its source. For these reasons, it is likely that study samples yielding lower and variable $\delta^{98}$Mo values reflect a fractionation process related to local redox conditions.

The fractionations recorded by LM samples with isotopically light $\delta^{98}$Mo may have been the result of either highly variable $[H_2S]_{aq}$ (i.e., fluctuating above and below this threshold) and/or influence of Fe-Mn shuttle (see above). If persistently low $[H_2S]_{aq}$ had existed during deposition of the LM, it should have resulted in relatively low Mo enrichments owing to the positive correlation of Mo uptake to $[H_2S]_{aq}$. In fact, the LM exhibits substantially greater Mo enrichment ($Mo_{EF} = 272 \pm 137$) than the UM ($61 \pm 22$) ($p < 0.01$), disproving the persistently low $[H_2S]_{aq}$ scenario. The alternative is highly variable $[H_2S]_{aq}$, with fluctuations at time scales shorter than the depositional interval of individual samples (mean ~ 20 kyr). In this scenario, intensely euxinic intervals alternated with less intensely reducing intervals (perhaps ranging from weakly euxinic to suboxic or oxic), with the former characterized by quantitative uptake by the sediment of Mo having the seawater $\delta^{98}$Mo composition, and the latter by more limited uptake of Mo having a composition fractionated to varying degrees toward lower $\delta^{98}$Mo values. The isotopically light LM samples thus represent a mixture of Mo fractions accumulating under variable redox conditions, whereas the isotopically heavy LM and UM samples represent inputs linked to persistently euxinic facies. The association of isotopically light samples with higher $Mo_{EF}$ values in the LM is somewhat unusual but consistent with Mo enrichment via a particulate shuttle linked to Fe-Mn cycling (see Section 6.2) (Cheng et al., 2016). In the next section, we consider the nature of redox fluctuations during deposition of the LM.

### 6.4. Transient oxygenation events

The nature of redox perturbations during deposition of the LM is revealed by detailed sedimentological observations. In the LM, multiple gray (i.e., lighter-colored) layers with thicknesses of ~1–2 mm have been observed (Fig. 2H). These gray layers show high corresponding to the appearance of sponge fossils and the lower $\delta^{98}$Mo. These layers likely record brief oxygenation episodes during which sufficient oxygen was supplied to the seafloor to permit transient colonization by sponges and other eukaryotes. Similar brief oxygenation episodes are known from anoxic marine sequences of many ages, including the Late Devonian (Algeo and Ingall, 2007), Early Jurassic (Kenig et al., 2004; Pearce et al., 2008), Cretaceous (Goldberg et al., 2016), Eocene (März et al., 2016), and modern (Algeo and Lyons, 2006; Jilbert and Slomp, 2013).

The development of transient oxygenation events may be reflected in certain aspects of the geochemistry of the study units. In Unit II, all samples with high $\delta^{98}$Mo (~+1.7‰) show higher $Fe_{py}$ (1.63±0.53%, $n = 8$) whereas those with lower $\delta^{98}$Mo show lower $Fe_{py}$ (0.63±0.24%, $n = 6$) ($p < 0.05$; Fig. 7A), suggesting a common redox control. Weathering processes can oxidize $Fe_{py}$ to $Fe_{ox}$ and preferentially leach isotopically heavier Mo (Pearce et al., 2010), but this process should lead to lower Mo concentrations, which is not observed in the study units (note that the $^{98}$Mo-depleted samples are associated with greater Mo enrichment; Fig. 3). Additionally, post-depositional weathering should lead to negative relationship between $Fe_{py}$ and $Fe_{ox}$, which is not observed in our samples too. Instead, a weak-to-moderate positive relationship is observed (Fig. 7B).

The observation that acquisition of a $^{98}$Mo-depleted signal accompanied higher Mo enrichment (Fig. 3) may be a key to understanding redox variations at Lantian. This pattern could develop in a dominantly anoxic environment (Fig. 8A) that was punctuated by brief oxygenation episodes (Fig. 8B) if local redox cycling of Fe-Mn particulates occurred at the seafloor during the oxygenation events (see Sections 6.2 and 6.3). $Mo^{6+}$ adsorption onto particulates occurs with a significant negative fractionation (Barling and Anbar, 2004), thus leading to $^{98}$Mo depletion of the Mo-enriched sediments. At the same time, under oxic conditions, microbial sulfate reduction was inhibited, resulting in less pyrite formation in the sediment (Li et al., 2015a).

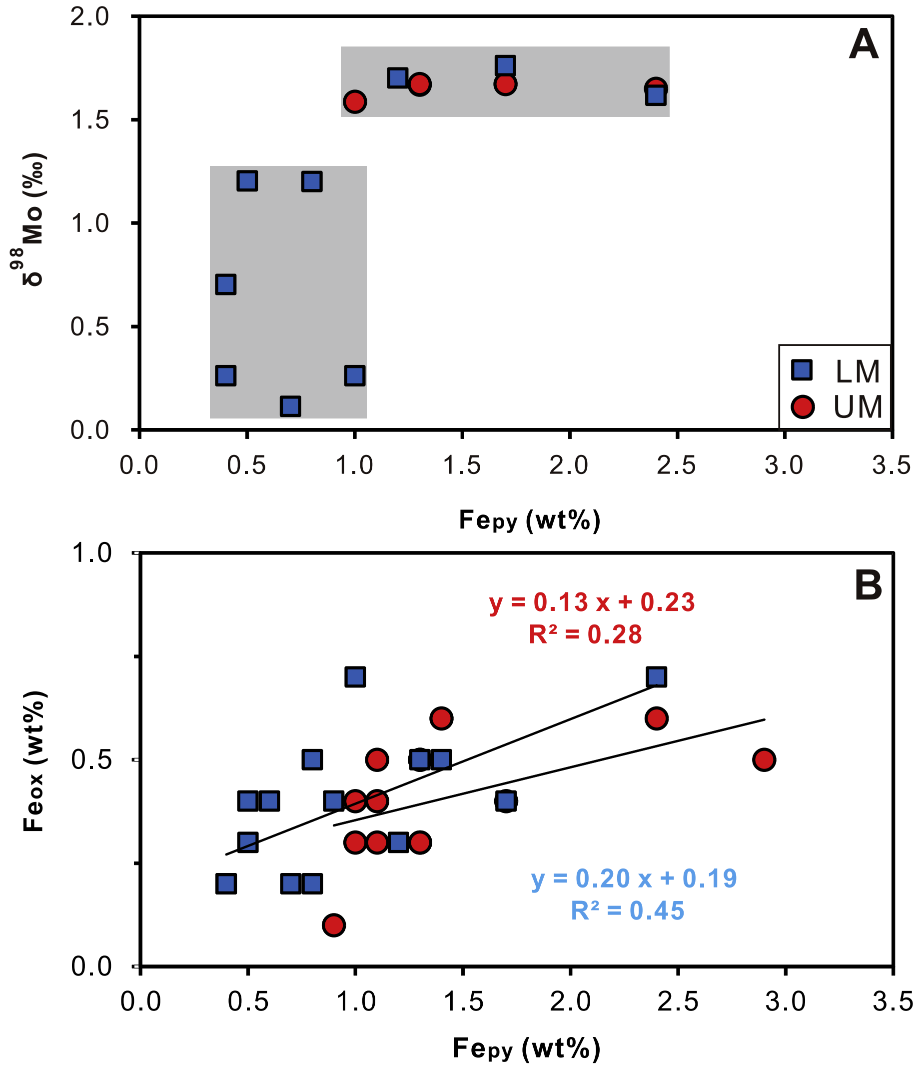


Fig. 7. (A) $\delta^{98}$Mo versus $Fe_{py}$, and (B) $Fe_{ox}$ versus $Fe_{py}$ for Unit II of the Hetang Formation in the Lantian section. LM = lower member, UM = upper member.

Thus, transient oxygenation events can explain concurrent low $Fe_{py}$ and light $\delta^{98}$Mo values (Fig. 7A). After complete consumption of benthic oxygen [probably over intervals of months to years by analogy with the modern Baltic Sea; (Jilbert and Slomp, 2013)], bottom waters would have returned to an anoxic condition but the sediment would have acquired higher RSTE/TOC ratios (Fig. 8C).

In summary, the transient development of oxic conditions in a dominantly anoxic environment during LM deposition is clearly demonstrated by lithologic and faunal evidence (i.e., lighter sediment color and sponge fossils) but only subtly by geochemical evidence (i.e., lower $Fe_{py}$, modestly elevated RSTE/TOC and lighter $\delta^{98}$Mo values). This pattern is linked to differences in response time of lithologic, faunal, and geochemical proxies for paleoredox conditions that came into play in a depositional system subject to high-frequency redox fluctuations. In contrast, the UM was characterized by stable, persistently euxinic local redox conditions that yielded relatively lower (but still enriched) RSTE concentrations and constant, higher $\delta^{98}$Mo values linked to local near-quantitative uptake of Mo from the water column (Fig. 8A). In this regard, the lack of any changes in sediment color or faunal content are consonant with the lack of short-term redox fluctuations during deposition of the UM.

Transient oxygenation events appear to have permitted temporary colonization by sponges of deep-water habitats at Lantian. As the simplest animals, the metabolism of sponges requires relatively low oxygen levels (Mills et al., 2014). Although the larger fossils in the LM can extend into the black layers, it is clear that the majority of sponge fossils are concentrated in the gray-colored layers (Fig. 2F–G), and, thus, that their distribution was strongly redox controlled. Sponges are commonly slow growing, possibly requiring years to decades to achieve a size up to ~1 m, as seen in the largest Hetang Biota sponges (Yuan et al., 2002), although some species, such as *Latrunculia wellingtonensis* and *Polymastia croceus*, are fast-growing (Maldonado et al., 2012). Transient oxygenation events in modern anoxic basins typically last from a few months to

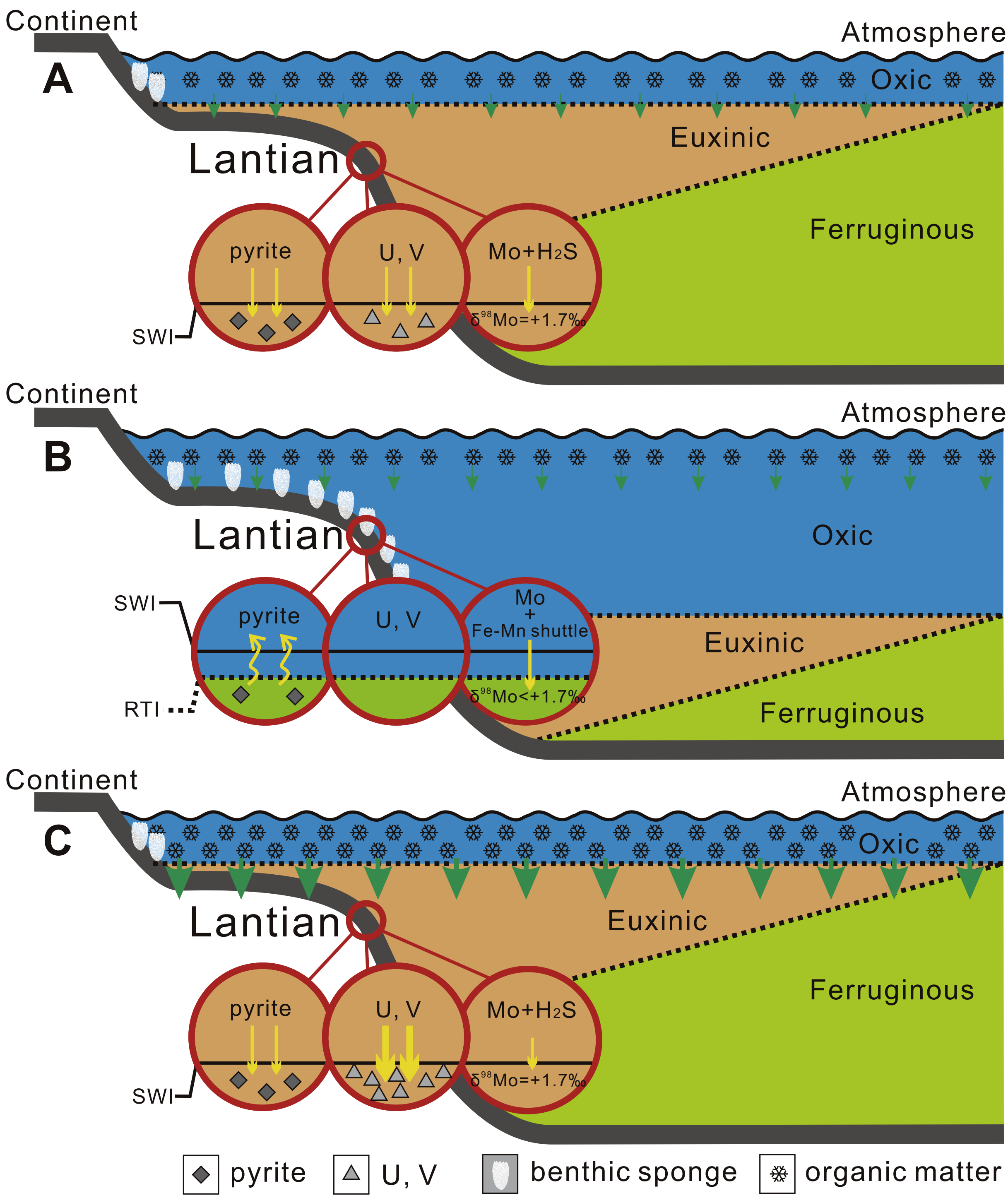


Fig. 8. Depiction of transient deep-water oxygenation events in the early Cambrian Nanhua Basin, South China, and their effects. (A) Background condition with anoxic deep waters. (B) Condition during an oxygenation event. (C) Condition following an oxygenation event. SWI = sediment water interface, RTI = redox transformation interface from oxic to anoxic condition.

a few years (Schinke and Matthäus, 1998), thus long enough for the appearance of sponge. Given an average sedimentation rate of 0.22 cm $kyr^{-1}$ (see Section 3), the time represented by the gray layers is estimated at ~0.5–1.0 kyr. This is, however, a maximum estimate because any downward penetration of oxygen from the sediment-water interface through either diffusion or bioturbation (which was limited in the early Cambrian) would have expanded the stratigraphic interval characterized as "gray shale". Similar occurrences of sponges in gray layers of the Hetang Formation and correlative units have been reported from other South China locales, e.g., Jinsha, Dingtai, Huangbailing and Wengan, although layer-to-layer correlation between these sections is not possible (cf. Jin et al., 2016). Sponges have also been reported from lower Cambrian black shales in Siberia, Greenland, and elsewhere globally (Botting and Peel, 2016). The wide occurrence of sponges in reducing facies of early Cambrian age suggests that the transient oxygenation events recorded in the Lantian section were not unique but, possibly, a manifestation of global-scale processes at that time. In addition, the faunas found at Lantian were typical of deep-water communities of this period (Botting and Peel, 2016), suggesting that deep-water oxygenation was an ongoing and spatially widespread process during the early Cambrian.

The exact mechanism by which oxygen was transferred into the deep-water environment at Lantian is unknown. Both bottom-hugging turbidites and density interflows can carry oxygen into deep basins as diffuse layers (Schmale et al., 2016), and vertical overturn can result in oxygenation of the full water column of a marine basin (McPhaden and Zhang, 2002). The stratigraphic pattern at Lantian, i.e., thin irregularly distributed gray shale layers, is most consistent with (although not proof of) oxygenation via distal turbidite flows. Given similar transient oxygenation events globally during the early Cambrian (see above), there is undoubtedly a global aspect to these occurrences. We hypothesize that rising oxygen levels in the atmosphere and ocean-surface layer at this time resulted in greater transfer of oxygen to deep-water setting by turbidites and density interflows, processes that would have operated regardless of ambient oxygen levels but that became more effective vectors of deepwater oxygenation as ocean-surface oxygen levels rose.

### 6.5. Differences in proxy response to high-frequency redox variation

The transient oxygenation events developed in the early Cambrian oceans cannot be tracked unless combining different proxies. The present study samples represent ~10–20 kyr of depositional time apiece (Section 3), far longer than the probable duration (<1 kyr) of any single oxygenation event (Section 6.4). Indeed some samples potentially record several such events that were closely spaced in time. The modern Baltic Sea provides an example of how frequent such redox fluctuations can be, with a total of ~96 transient oxygenation events during the 20th century (Schinke and Matthäus, 1998). As a consequence, individual sample potentially came under the influence of widely varying redox conditions (e.g., from oxic to euxinic) during their accumulation. In such situations, multiple types of proxies can yield quite different redox indications, as in the present study. Similar effects have been reported for other anoxic paleomarine systems subject to brief oxygenation episodes. For example, in Jurassic Toarcian shales, bioturbation is found juxtaposed with organic geochemical proxies indicating euxinia (Kenig et al., 2004). In Cretaceous OAE2 sediments, bioturbation is found in beds for which iron speciation data indicate persistently anoxic conditions (Goldberg et al., 2016). In each of these cases, temporally brief oxygenation events appear to have had no measurable effect on geochemical proxies recording the dominant (i.e., anoxic) redox signal.

The sensitivities to transient redox perturbations of benthic fauna, iron species, RSTEs, and Mo isotopes are quite different. In the LM, sponges appear mainly in three layers whereas Mo isotopes show more frequent negative excursions (Fig. 3). This suggests that Mo isotopes may be recording transient oxygenation events in which oxygen levels did not rise high enough to permit colonization of the seafloor by a benthic fauna. This pattern is consistent with the idea that Mo isotopes are affected when $[H_2S]_{aq}$ is below a critical threshold value and/or by the Fe-Mn shuttle, suggesting that a combination of reduced $\delta^{98}$Mo values and lack of benthic fauna is indicative of weakly euxinic to suboxic conditions. TOC and $Fe_{py}/Fe_{HR}$ show more limited sample-to-sample variation in the LM than $\delta^{98}$Mo, but the LM nonetheless shows significantly different mean values from the UM (Fig. 3). TOC and iron species are controlled by local- to basin-scale productivity and iron fluxes as well as benthic redox conditions. RSTEs (Mo, U and V) show some differences in their vertical profiles (Fig. 3), reflecting differential responses to specific redox conditions. For example, uptake of authigenic Mo requires the presence of $H_2S$, but uptake of authigenic U requires only that the $Fe^{3+}/Fe^{2+}$ transition has occurred (i.e., suboxic conditions), and V exhibits a complex two-step pattern of enrichment with progressively more reducing conditions (Algeo and Maynard, 2004; Tribovillard et al., 2006). By making use of multiple proxies, it should be possible to refine evaluations of redox conditions in ancient marine systems. For these reasons, we recommend the standard application of multiple proxies in paleoceanographic studies.

## 7. CONCLUSIONS

To explore apparent conflicts of redox interpretations between fossil and geochemical evidence in the lower Cambrian Hetang Formation (~535–521 Ma) at Lantian (Nanhua Basin, South China), we analyzed Mo isotopes, iron species, and RSTEs in relation to benthic faunal occurrences. Although $Fe_{HR}/Fe_T$ >0.38 throughout the study interval indicates a persistently anoxic depositional environment, RSTE/TOC ratios and Mo isotopes show considerable variation, with higher RSTE/TOC and lower $\delta^{98}$Mo associated with gray (lighter-colored) sponge-bearing layers. This pattern indicates the episodic development of brief (<1 kyr) oxygenation events in the normally anoxic early Cambrian Nanhua Basin. Transient ventilation of the deep basin floor permitted colonization by sponges and may have enhanced authigenic Mo through small-scale Mn-Fe redox cycling at the sediment–water interface which resulted in the lower $\delta^{98}$Mo values. Our study thus provides direct evidence of transient oxygenation events in anoxia-dominated early Cambrian oceans. The study units show markedly differential responses of the various proxies used here (benthic fauna, Mo isotopes, iron species, and RSTEs) to high-frequency redox fluctuations that probably ranged from mildly oxic to strongly euxinic. Such differential responses potentially provide a basis for more refined evaluation of redox conditions in paleomarine systems.

## ACKNOWLEDGMENTS

We thank Shi-Da Tang, Zhi-Fang Hu and Lan-Ping Feng for laboratory assistance, and Hai-Yang Wang and Na Li for their useful discussions. We also appreciate the comments from the editor (Nicolas Dauphas) and two anonymous reviewers, which greatly improved this manuscript. This study was supported by the Chinese 973 program (Grant 2013CB955704), NSFC-RCUK_NERC Program (Grant 41661134048), the NSFC (Grant 41172030), the 111 Project (Grant B08030), GPMR-CUG (Grant GPMR201705) and Fundamental Research Funds for Central Universities (CUG-Wuhan; Grant 1610491T01 and G1323531767). Lian Zhou acknowledges funding by the NSFC (Grants 41473007, 41673013). Shao-Yong Jiang acknowledges funding by NSFC (Grant 41230102). Thomas Algeo acknowledges funding by the U.S. NASA Exobiology program.

## REFERENCES

Algeo T. J. (2004) Can marine anoxic events draw down the trace element inventory of seawater? *Geology* **32**, 1057–1060.

Algeo T. J. and Ingall E. (2007) Sedimentary Corg: P ratios, paleocean ventilation, and phanerozoic atmospheric pO2. *Palaeogeogr. Palaeoclimatol. Palaeoecol.* **256**, 130–155.

Algeo T. J., Luo G. M., Song H. Y., Lyons T. W. and Canfield D. E. (2015) Reconstruction of secular variation in seawater sulfate concentrations. *Biogeosciences* **12**, 2131–2151.

Algeo T. J. and Lyons T. W. (2006) Mo-total organic carbon covariation in modern anoxic marine environments: Implications for analysis of paleoredox and paleohydrographic conditions. *Paleoceanography* **21**. http://dx.doi.org/10.1029/2004pa001112.

Algeo T. J. and Maynard J. B. (2004) Trace-element behavior and redox facies in core shales of Upper Pennsylvanian Kansas-type cyclothems. *Chem. Geol.* **206**, 289–318.

Algeo T. J. and Rowe H. (2012) Paleoceanographic applications of trace-metal concentration data. *Chem. Geol.* **324–325**, 6–18.

Algeo T. J. and Tribovillard N. (2009) Environmental analysis of paleoceanographic systems based on molybdenum–uranium covariation. *Chem. Geol.* **268**, 211–225.

Arnold G. L., Anbar A. D., Barling J. and Lyons T. W. (2004) Molybdenum isotope evidence for widespread anoxia in mid-Proterozoic oceans. *Science* **304**, 87–90.

Arnold G. L., Lyons T. W., Gordon G. W. and Anbar A. D. (2012) Extreme change in sulfide concentrations in the black sea during the little ice age reconstructed using molybdenum isotopes. *Geology* **40**, 595–598.

Barling J. and Anbar A. D. (2004) Molybdenum isotope fractionation during adsorption by manganese oxides. *Earth Planet. Sci. Lett.* **217**, 315–329.

Botting, J.P., Peel, J.S., 2016. Early Cambrian sponges of the Sirius Passet Biota, North Greenland. Papers in Palaeontology.

Breillat N., Guerrot C., Marcoux E. and Négrel P. (2016) A new global database of δ 98 Mo in molybdenites: a literature review and new data. *J. Geochem. Explor.* **161**, 1–15.

Canfield D. E., Poulton S. W., Knoll A. H., Narbonne G. M., Ross G., Goldberg T. and Strauss H. (2008) Ferruginous conditions dominated later neoproterozoic deep-water chemistry. *Science* **321**, 949–952.

Canfield D. E., Raiswell R., Westrich J. T., Reaves C. M. and Berner R. A. (1986) The use of chromium reduction in the analysis of reduced inorganic sulfur in sediments and shales. *Chem. Geol.* **54**, 149–155.

Chen X., Ling H. F., Vance D., Shields-Zhou G. A., Zhu M., Poulton S. W., Och L. M., Jiang S. Y., Li D., Cremonese L. and Archer (2015) Rise to modern levels of ocean oxygenation coincided with the Cambrian radiation of animals. *Nat. Commun.* **6**, 7142.

Cheng M., Li C., Zhou L., Algeo T. J., Zhang F., Romaniello S., Jin C.-S., Lei L.-D., Feng L.-J. and Jiang S.-Y. (2016) Marine Mo biogeochemistry in the context of dynamically euxinic mid-depth waters: A case study of the lower Cambrian Niutitang shales, South China. *Geochim. Cosmochim. Acta* **183**, 79–93.

Cheng M., Li C., Zhou L. and Xie S. C. (2015) Mo marine geochemistry and reconstruction of ancient ocean redox states. *Sci. China-Earth Sci.* **58**, 2123–2133.

Clarkson M. O., Poulton S. W., Guilbaud R. and Wood R. A. (2014) Assessing the utility of Fe/Al and Fe-speciation to record water column redox conditions in carbonate-rich sediments. *Chem. Geol.* **382**, 111–122.

Dahl T. W., Chappaz A., Fitts J. P. and Lyons T. W. (2013) Molybdenum reduction in a sulfidic lake: Evidence from X-ray absorption fine-structure spectroscopy and implications for the Mo paleoproxy. *Geochim. Cosmochim. Acta* **103**, 213–231.

Dahl T. W., Hammarlund E. U., Anbar A. D., Bond D. P. G., Gill B. C., Gordon G. W., Knoll A. H., Nielsen A. T., Schovsbo N. H. and Canfield D. E. (2010) Devonian rise in atmospheric oxygen correlated to the radiations of terrestrial plants and large predatory fish. *Proc. Natl. Acad. Sci. U. S. A.* **107**, 17911–17915.

Erickson B. E. and Helz G. R. (2000) Molybdenum(VI) speciation in sulfidic waters: Stabiloty and lability of thiomolybdates. *Geochim. Cosmochim. Acta* **64**, 1149–1158.

Feng L., Li C., Huang J., Chang H. and Chu X. (2014) A sulfate control on marine mid-depth euxinia on the early Cambrian (ca. 529–521 Ma) Yangtze platform, South China. *Precambr. Res.* **246**, 123–133.

Goldberg T., Gordon G., Izon G., Archer C., Pearce C. R., McManus J., Anbar A. D. and Rehkämper M. (2013) Resolution of inter-laboratory discrepancies in Mo isotope data: an intercalibration. *J. Annal. Atom. Spectrom.* **28**, 724–735.

Goldberg T., Poulton S. W., Wagner T., Kolonic S. F. and Rehkämper M. (2016) Molybdenum drawdown during cretaceous oceanic anoxic event 2. *Earth Planet. Sci. Lett.* **440**, 81–91.

Goldberg T., Strauss H., Guo Q. and Liu C. (2007) Reconstructing marine redox conditions for the early Cambrian yangtze platform: evidence from biogenic sulphur and organic carbon isotopes. *Palaeogeogr. Palaeoclimatol. Palaeoecol.* **254**, 175–193.

Gordon G. W., Lyons T. W., Arnold G. L., Roe J., Sageman B. B. and Anbar A. D. (2009) When do black shales tell molybdenum isotope tales? *Geology* **37**, 535–538.

Grice K., Cao C., Love G. D., Bottcher M. E., Twitchett R. J., Grosjean E., Summons R. E., Turgeon S. C., Dunning W. and Jin Y. (2005) Photic zone euxinia during the Permian-triassic superanoxic event. *Science* **307**, 706–709.

Guan C., Zhou C., Wang W., Wan B., Yuan X. and Chen Z. (2014) Fluctuation of shelf basin redox conditions in the early Ediacaran: Evidence from Lantian Formation black shales in South China. *Precambr. Res.* **245**, 1–12.

Jiang G., Kennedy M. J. and Christie-Blick N. (2003) Stable isotopic evidence for methane seeps in Neoproterozoic post-glacial cap carbonates. *Nature* **426**, 822–826.

Jilbert T. and Slomp C. P. (2013) Rapid high-amplitude variability in Baltic Sea hypoxia during the Holocene. *Geology* **41**, 1183–1186.

Jin C., Li C., Algeo T. J., Planavsky N. J., Cui H., Yang X., Zhao Y., Zhang X. and Xie S. (2016) A highly redox-heterogeneous ocean in South China during the early Cambrian (∼529–514 Ma): Implications for biota-environment co-evolution. *Earth Planet. Sci. Lett.* **441**, 38–51.

Kendall B., Komiya T., Lyons T. W., Bates S. M., Gordon G. W., Romaniello S. J., Jiang G. Q., Creaser R. A., Xiao S. H., McFadden K., Sawaki Y., Tahata M., Shu D. G., Han J., Li Y., Chu X. L. and Anbar A. D. (2015) Uranium and molybdenum isotope evidence for an episode of widespread ocean oxygenation during the late Ediacaran Period. *Geochim. Cosmochim. Acta* **156**, 173–193.

Kenig F., Hudson J. D., Sinninghe Damsté J. S. and Popp B. N. (2004) Intermittent euxinia: Reconciliation of a Jurassic black shale with its biofacies. *Geology* **32**, 421.

Knoll A. H. and Carroll S. B. (1999) Early animal evolution: Emerging views from comparative biology and geology. *Science* **284**, 2129–2137.

Large R. R., Halpin J. A., Danyushevsky L. V., Maslennikov V. V., Bull S. W., Long J. A., Gregory D. D., Lounejeva E., Lyons T. W., Sack P. J., McGoldrick P. J. and Calver C. R. (2014) Trace element content of sedimentary pyrite as a new proxy for deep-time ocean–atmosphere evolution. *Earth Planet. Sci. Lett.* **389**, 209–220.

Li C., Cheng M., Algeo T. J. and Xie S. (2015a) A theoretical prediction of chemical zonation in early oceans (>520 Ma). *Sci. China-Earth Sci.* **58**, 1901–1909.

Li C., Love G. D., Lyons T. W., Fike D. A., Sessions A. L. and Chu X. (2010) A stratified redox model for the Ediacaran ocean. *Science* **328**, 80–83.

Li C., Love G. D., Lyons T. W., Scott C. T., Feng L., Huang J., Chang H., Zhang Q. and Chu X. (2012) Evidence for a redox stratified Cryogenian marine basin, Datangpo Formation, South China. *Earth Planet. Sci. Lett.* **331–332**, 246–256.

Li C., Planavsky N. J., Shi W., Zhang Z., Zhou C., Cheng M., Tarhan L. G., Luo G. and Xie S. (2015b) Ediacaran marine redox heterogeneity and early animal ecosystems. *Sci. Rep.* **5**, 17097.

Lyons T. W. and Severmann S. (2006) A critical look at iron paleoredox proxies: New insights from modern euxinic marine basins. *Geochim. Cosmochim. Acta* **70**, 5698–5722.

Maldonado M., Ribes M. and van Duyl F. C. (2012) Nutrient fluxes through sponges: biology, budgets, and ecological implications. *Adv. Mar. Biol.* **62**, 113–182.

März C., Wagner T., Aqleh S., Al-Alaween M., van den Boorn S., Podlaha O. G., Kolonic S., Poulton S. W., Schnetger B. and Brumsack H. J. (2016) Repeated enrichment of trace metals and organic carbon on an Eocene high-energy shelf caused by anoxia and reworking. *Geology* **44**, 1011–1014.

McLennan S. M. (2001) Relationships between the trace element composition of sedimentary rocks and upper continental crust. *Geochem. Geophys. Geosyst.* **2**. http://dx.doi.org/10.1029/2000GC000109.

McPhaden M. J. and Zhang D. (2002) Slowdown of the meridional overturning circulation in the upper Pacific ocean. *Nature* **415**, 603–608.

Mills D. B., Ward L. M., Jones C., Sweeten B., Sweeten M., Forth M., Alexander H. T. and Canfield D. E. (2014) Oxygen requirements of the earliest animals. *Proc. Natl. Acad. Sci. U. S. A.* **111**, 4168–4172.

Moya A., Pereto J., Gil R. and Latorre A. (2008) Learning how to live together: genomic insights into prokaryote-animal symbioses. *Nat. Rev. Genet.* **9**, 218–229.

Nägler T. F., Anbar A. D., Archer C., Goldberg T., Gordon G. W., Greber N. D., Siebert C., Sohrin Y. and Vance D. (2013) Proposal for an international molybdenum isotope measurement standard and data representation. *Geostand. Geoanal. Res.* **38**, 149–151.

Neubert N., Nägler T. F. and Böttcher M. E. (2008) Sulfidity controls molybdenum isotope fractionation into euxinic sediments: Evidence from the modern Black Sea. *Geology* **36**, 775–778.

Pearce C. R., Burton K. W., Pogge von Strandmann P. A. E., James R. H. and Gislason S. R. (2010) Molybdenum isotope behaviour accompanying weathering and riverine transport in a basaltic terrain. *Earth Planet. Sci. Lett.* **295**, 104–114.

Pearce C. R., Cohen A. S., Coe A. L. and Burton K. W. (2008) Molybdenum isotope evidence for global ocean anoxia coupled with perturbations to the carbon cycle during the Early Jurassic. *Geology* **36**, 231–234.

Poulson R. L., Siebert C., Mcmanus J. and Berelson W. M. (2006) Authigenic molybdenum isotope signatures in marine sediments. *Geology* **34**(8), 617. http://dx.doi.org/10.1130/G22485.1.

Poulton S. and Canfield D. (2005) Development of a sequential extraction procedure for iron: implications for iron partitioning in continentally derived particulates. *Chem. Geol.* **214**, 209–221.

Poulton S. W. and Canfield D. E. (2011) Ferruginous conditions: A dominant feature of the ocean through Earth's history. *Elements* **7**, 107–112.

Raiswell R. and Canfield D. E. (2012) The iron biogeochemical cycle past and present. *Geochem. Perspect.* **1**, 1–220.

Reinhard C. T., Planavsky N. J., Robbins L. J., Partin C. A., Gill B. C., Lalonde S. V., Bekker A., Konhauser K. O. and Lyons T. W. (2013) Proterozoic ocean redox and biogeochemical stasis. *Proc. Natl. Acad. Sci. U. S. A.* **110**, 5357–5362.

Schinke H. and Matthäus W. (1998) On the causes of major Baltic inflows —an analysis of long time series. *Cont. Shelf Res.* **18**, 67–97.

Schmale O., Krause S., Holtermann P., Power Guerra N. C. and Umlauf L. (2016) Dense bottom gravity currents and their impact on pelagic methanotrophy at oxic/anoxic transition zones. *Geophys. Res. Lett.* **43**, 5225–5232.

Scholz F., Löscher C. R., Fiskal A., Sommer S., Hensen C., Lomnitz U., Wuttig K., Göttlicher J., Kossel E., Steininger R. and Canfield D. E. (2016) Nitrate-dependent iron oxidation limits iron transport in anoxic ocean regions. *Earth Planet. Sci. Lett.*.

Scott C. and Lyons T. W. (2012) Contrasting molybdenum cycling and isotopic properties in euxinic versus non-euxinic sediments and sedimentary rocks: Refining the paleoproxies. *Chem. Geol.* **324**, 19–27.

Scott C., Lyons T. W., Bekker A., Shen Y., Poulton S. W., Chu X. and Anbar A. D. (2008) Tracing the stepwise oxygenation of the Proterozoic ocean. *Nature* **452**, 456–459.

Siebert C., Nägler T. F., von Blanckenburg F. and Kramers J. D. (2003) Molybdenum isotope records as a potential new proxy for paleoceanography. *Earth Planet. Sci. Lett.* **211**, 159–171.

Sperling E. A., Knoll A. H. and Girguis P. R. (2015a) The ecological physiology of earth's second oxygen revolution. *Annu. Rev. Ecol. Evol. Syst.* **46**, 215–235.

Sperling E. A., Wolock C. J., Morgan A. S., Gill B. C., Kunzmann M., Halverson G. P., Macdonald F. A., Knoll A. H. and Johnston D. T. (2015b) Statistical analysis of iron geochemical data suggests limited late Proterozoic oxygenation. *Nature* **523**, 451–454.

Tessin A., Sheldon N. D., Hendy I. and Chappaz A. (2016) Iron limitation in the western interior seaway during the late cretaceous OAE 3 and its role in phosphorus recycling and enhanced organic matter preservation. *Earth Planet. Sci. Lett.* **449**, 135–144.

Tribovillard N., Algeo T. J., Lyons T. and Riboulleau A. (2006) Trace metals as paleoredox and paleoproductivity proxies: An update. *Chem. Geol.* **232**, 12–32.

Voegelin A. R., Pettke T., Greber N. D., von Niederhäusern B. and Nägler T. F. (2014) Magma differentiation fractionates Mo isotope ratios: Evidence from the Kos Plateau Tuff (Aegean Arc). *Lithos* **190–191**, 440–448.

Wang J. and Li Z. X. (2003) History of neoproterozoic rift basins in South China: implications for Rodinia break-up. *Precambr. Res.* **122**, 141–158.

Wignall P. B. and Twitchett R. J. (1996) Oceanic anoxia and the end Permian mass extinction. *Science* **272**, 1155–1158.

Wille M., Nägler T. F., Lehmann B., Schröder S. and Kramers J. D. (2008) Hydrogen sulphide release to surface waters at the Precambrian/Cambrian boundary. *Nature* **453**, 767–769.

Xiao S., Hu J., Yuan X., Parsley R. L. and Cao R. (2005) Articulated sponges from the Lower Cambrian Hetang Formation in southern Anhui, South China: their age and implications for the early evolution of sponges. *Palaeogeogr. Palaeoclimatol. Palaeoecol.* **220**, 89–117.

Yang J., Barling J., Siebert C., Fietzke J., Stephens E. and Halliday A. N. (2017) The molybdenum isotopic compositions of I-, S- and A-type granitic suites. *Geochim. Cosmochim. Acta* **205**, 168–186.

Yuan X., Chen Z., Xiao S., Zhou C. and Hua H. (2011) An early Ediacaran assemblage of macroscopic and morphologically differentiated eukaryotes. *Nature* **470**, 390–393.

Yuan X., Xiao S., Parsley R. L., Zhou C. and Hu J. (2002) Towering sponges in an Early Cambrian Lagerstatte: Disparity between nonbilaterian and bilaterian epifaunal tierers at the Neoperozoic-Cambrian trasition. *Geology* **30**, 363–366.

Zhang S., Li H., Jiang G., Evans D. A. D., Dong J., Wu H., Yang T., Liu P. and Xiao Q. (2015) New paleomagnetic results from the Ediacaran Doushantuo Formation in South China and their paleogeographic implications. *Precambr. Res.* **259**, 130–142.

Zhang X. and Cui L. (2016) Oxygen requirements for the Cambrian explosion. *J. Earth Sci.* **27**, 187–195.

Zhou C. and Jiang S.-Y. (2009) Palaeoceanographic redox environments for the lower Cambrian Hetang Formation in South China: Evidence from pyrite framboids, redox sensitive trace elements, and sponge biota occurrence. *Palaeogeogr. Palaeoclimatol. Palaeoecol.* **271**, 279–286.

*Associate editor:* Nicolas Dauphas